Poly(ϵ-caprolactone)−Clay Nanocomposites: Structure and Mechanical Properties

Biqiong Chen and Julian R. G. Evans*

Department of Materials, Queen Mary, University of London, Mile End Road, London E1 4NS, United Kingdom

Received October 5, 2005; Revised Manuscript Received November 18, 2005

ABSTRACT: The modulus−volume fraction relationship for a poly(ϵ-caprolactone)−montmorillonite nanocomposite follows composite materials theory provided the clay volume fraction is correctly calculated. Thus, for interpretation of mechanical properties, nanocomposites do not have to be treated as a separate class of material. The tensile modulus of biodegradable poly(ϵ-caprolactone) was increased by 50% at 8 wt % clay addition (as corrected for surfactant), but the more dramatic improvement was in tensile elongation at break which increased from 165% to 550% for additions of up to 10 wt % clay. Poly(ϵ-caprolactone) nanocomposites with various clay volume fractions were produced with two organo-modified montmorillonites. Untreated montmorillonite was used as an experimental control to compare the properties with a conventional composite over the same clay volume fraction range, The composites were confirmed and characterized by XRD, DSC, NMR, and TEM.

Introduction

Following the success of nylon−montmorillonite nanocomposites in motor vehicle applications,[1−3] there has been a rapid expansion of interest in different smectite clay−polymer systems with the aim of producing enhanced mechanical, barrier, and electrical properties yet retaining a wide range of processing options. These efforts, which draw upon decades of careful study of organic interactions in clays,[4−6] are beginning to provide effective composites from relatively humble and often ignored materials resources.

Biodegradable polymers such as poly(ϵ-caprolactone) (PCL), starch, and poly(lactide) (PLA) are of interest in disposable packaging applications on environmental grounds. However, the applications for such polymers are limited because of their deficiencies in mechanical and barrier properties to water and gases. One option is to incorporate an environmentally acceptable filler to improve the properties of such biodegradable polymers particularly for use as packaging materials. Clay is a suitable filler—itself a naturally abundant mineral that is toxin-free and can be used as one of the components for food, medical, cosmetic, and health-care recipients.[7−9] Indeed, biodegradable polymers reinforced by clay are now being investigated.[10−16] Such nanocomposites are prepared by direct melt-intercalation, by solvent intercalation, and by in situ polymerization, of which the first is the main method. This work focuses on PCL−clay composites prepared using melt processing.

Lepoittevin et al.[10] melt processed PCL−organoclay nanocomposites using a twin roll mill; hydrophobic PCL forms conventional composites with natural smectite clays but forms nanocomposites with organophilic ammonium-treated clays.[11,12] The ammonium-treated clay had increased mechanical strength and modulus, decreased gas and water permeability, and increased biodegradability. For example, Young's modulus of PCL was increased from 216 to 390 MPa with 10 wt % ammonium-treated montmorillonite.[12] In another study, Young's modulus was increased from 120 to 445 MPa with 9 wt % ammonium-treated clay.[11−13] Meanwhile, the zero-concentration diffusion coefficient of water vapor for PCL was significantly decreased from 2.36×10^{-4} to 1.07×10^{-4} m^2 s^{-1}. PCL was also found to form char in the presence of clay when exposed to a flame, without forming liquid droplets. Charring occurred with deposition of solid residue on the surface, which provides PCL nanocomposites with fire-retardant properties.[10]

This work sets out to prepare conventional and nanocomposite PCL−clay systems, each with a range of clay volume fractions, in order to assess the structure and to examine systematic trends in the enhancement of mechanical properties.

Experimental Details

Three types of montmorillonite were used as reinforcement for a commercial poly(ϵ-caprolatone) to provide composites of different types. Natural sodium montmorillonite (type: BH natural, denoted as MMT) was from Blackhill Bentonite LLC (Wyoming). Two montmorillonite clays modified with 2-methyl-2-hydrogenated tallow quaternary ammonium chloride (type: bentone 105, denoted as NH_4MMT1) and a benzyl-2-methyl-hydrogenated tallow quaternary ammonium chloride (type: bentone 111, denoted as NH_4-MMT2) were from Elementis Specialties (Hightstown, NJ). PCL with number-average molecular weight of 80 000 was from Sigma-Aldrich Chemicals. All materials were used without further modification.

The composites were prepared by melt-processing. Preweighed amounts of clay were gradually added to PCL melt on a heated twin roll mill (Carter International, Rochdale, UK). The mixture was stripped from the rolls and refed at least five times to ensure lateral mixing. The average processing temperature was 128 °C. Exact composition was deduced from loss on ignition. Four crucibles with ∼2.7 g composites were heated to 600 °C at 10 °C min^{-1} in a muffle furnace (Lenton Thermal Design Ltd., Sheffield, UK) and after a dwell of 600 s furnace-cooled to 20 °C. The residue was weighed after storing in air at 20 °C for 8 h. As-received clays were also fired and weighed to correct for water loss.

A Siemens D5000 X-ray diffractomer (40 kV, 40 mA) equipped with a graphite monochromator and with Cu $K\alpha_1$ radiation (λ = 0.154 06 nm) was used for X-ray diffraction (XRD) of the composites. The aperture slits were set as 0.1°, and the scanning step was 0.02° with a scan time of 2.5 s per step. The specimens were prepared using a hydraulic press, and measurements were conducted on samples with parallel surfaces. Differential scanning calorimetry (DSC) was conducted on a Perkin-Elmer DSC 7

* To whom correspondence should be addressed: e-mail j.r.g.evans@qmul.ac.uk; Tel 0044 20 7882 5501; Fax 0044 20 8981 9804.

10.1021/ma052154a CCC: $33.50
Published on Web 12/24/2005

Scheme 1. Chemical Structure of 2-Methyl-2-hydrogenated Tallow Quaternary Ammonium

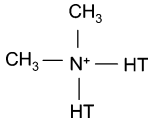

Scheme 2. Chemical Structure of Benzyl-2-methyl-hydrogenated Tallow Quaternary Ammonium

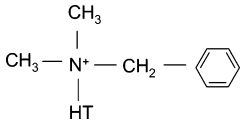

instrument. The specimens were contained in aluminum crucibles and heated at 3 °C min^{-1} from 25 °C in a nitrogen gas flow rate of 20 mL min^{-1}.

Scanning electron microscopy (SEM) on fracture surfaces was performed on a JEOL JSM6300 with an operating voltage at 10 kV. All the specimens were sputter-coated with gold. Transmission electron microscopy (TEM) was conducted on a JEOL JEM2010 electron microscope, operating at 200 kV, and with Kodak SO-163 film. TEM specimens were prepared by ultramicrotoming pretrimmed nanocomposite blocks with a diamond knife on a Reichert Om U2 microtome (Reichert Ophthalmic Instruments, New York) at room temperature to give sections with thickness less than 100 nm. The sections were transferred from water to 400 mesh copper grids. Solid-state NMR was conducted at ambient temperature on a Bruker AV600 spectrometer operating at 600 MHz. Typically about 100 mg was used to fill the MAS rotor. The MAS spinning rate was 10 000 Hz, the 90° pulse width was 3.7 μs, and the ramped CP pulse was 1 ms. TPPM15 decoupling of ^{1}H was used, and the ^{1}D spectrum of ^{13}C was run with spinning sideband suppression according to Dixon et al.[17]

Elastic constants of polymer−clay nanocomposites were calculated from ultrasonic measurements in the pulse-echo mode using a 500PR ultrasonic pulser/receiver (Panametrics NDT Ltd., Rotherham, UK) and a TDS200 digital real-time oscilloscope (Tektronix, Beaverton, OR). Measurements were calibrated with a surface-ground steel step-wedge. Flat parallel-faced specimens were prepared on a hot press.

Tensile and flexural tests were carried out on an Instron 5564 using a 1 kN load cell according to ASTM D638M and ASTM D6272, respectively. For tensile testing, an extensometer was fitted at low elongations. The specimens were dumbbell shaped with dimensions of type III (60 mm × 10 mm × 4 mm). The rate of cross-head motion was 5 mm min^{-1} with the extensometer fitted and 50 mm min^{-1} thereafter. Four-point flexural test specimens had dimensions of 80 mm × 10 mm × 4 mm, and the cross-head speed was 17 mm min^{-1}, the tests being terminated at 5% strain according to the standard. The flexural modulus was measured with an extensometer. All test specimens were molded using a small injection-molding machine (Ray-ran Test Equipment Ltd., Nuneaton, UK) operated at 0.9 MPa with barrel temperature and mold temperature of 115 and 40 °C, respectively.

Results and Discussion

(i) Characterization and Property Enhancement. Conventional PCL−clay composites were produced from natural montmorillonite, but nanocomposites with different degrees of intercalation were obtained from the two ammonium-treated montmorillonites. Chemical structures of the two modifiers are shown in Schemes 1 and 2 where HT refers to hydrogenated tallow.

The compositions of PCL−clay composites deduced from loss on ignition are shown in Table 1. The largest clay loading (58.5 wt %) was not the maximum amount that PCL could sustain, suggesting that the PCL with a molecular weight of 80 000 can at least sustain a similar loading of clay to poly(ethylene oxide) with a molecular weight of 100 000 previously investigated (64 wt %).[18]

Table 1. Compositions of PCL−Clay Composites Deduced from Loss on Ignition

sample ID[e]	wt % of clay platelet	wt % of clay	effective vol % of clay
MMT	93.8	100	
M2[a,b]	1.6	1.7	0.8
M4	3.7	3.9	1.8
M11	10.7	11.4	5.4
M20	19.9	21.2	10.6
M34	33.9	36.2	20.0
M45	44.6	47.5	28.5
M55	54.8	58.5	38.3
NH_4MMT1	62.2	100	
1NM1[b,c]	1.1	1.8	1.4
1NM1b	1.2	2.0	1.5
1NM4	4.2	6.8	5
1NM8	8.2	13.1	10
1NM16	16.3	26.2	21
1NM24	23.9	38.4	33
1NM30	29.9	48.2	42
NH_4MMT2	77.8	100	
2NM2[b,d]	2.2	2.9	3
2NM3	2.9	3.7	4
2NM7	6.8	8.8	10
2NM12	11.9	15.3	18
2NM19	18.7	24.1	28
2NM29	29.1	37.4	37
2NM33	32.8	42.2	42

[a] M = PCL−MMT composite. [b] The numbers in MX and NMX refer to nominal weight percent of clay platelets. [c] 1NM = PCL−NH_4MMT1 nanocomposite. [d] 2NM = PCL−NH_4MMT2 nanocomposite. [e] The nomenclature is used throughout this article.

XRD traces of the PCL−clay composites are shown in Figure 1. PCL did not intercalate into natural montmorillonite, as deduced from the unchanged d_{001} after melt-processing (Figure 1a). Both ammonium-treated montmorillonites produced PCL−clay nanocomposites according to the increase in d_{001}, which agrees with the findings of Lepoittevin et al.[10] and Gorrasi et al.[12] PCL is a hydrophobic polymer and is only compatible with "organophilic" clays. Figure 1b shows that the (001) peak of NH_4MMT1 shifted consistently from 2.88° of 2θ to 2.5° even with different clay loadings, corresponding to an increase of d_{001} of 3.1−3.5 nm. It could be argued that this is due to a rearrangement of surfactant molecules in the galleries rather than intercalation, but when as-received NH_4MMT1 alone was subjected to the same heating conditions, d_{001} underwent a slight decrease (0.3 nm). The increase of 0.4 nm is equivalent to a monolayer of PCL molecules if the intercalated polymer only occupies the increased spacing of treated clays as supposed by Okada et al.[2] and LeBaron et al.[6]

In the case of NH_4MMT2, the initial (001) peak at 4.4° (corresponding to d_{001} = 2.0 nm) was gradually replaced by the appearance of a peak at 3.6 nm, but when the clay content was greater than 37.4 wt %, d_{001} was replaced by a peak at 2.8 nm; otherwise, d_{001} was 3.6 nm. If a planar conformation is assumed, these two values of d_{001} correspond to a planar bilayer and a "quadlayer" of PCL molecules lying in the galleries of the treated clay on the basis that a planar monolayer is often taken as 0.4 nm.[19,20] With less clay, it appears that there is sufficient polymer availability and mobility to develop a greater gallery height. When the suspension is crowded, polymer molecules may be restricted by adsorption on adjacent sites, resulting only in a bilayer. To ascertain the conformation of the intercalated PCL needs other techniques such as NMR and modeling work because PCL could indeed adopt helical[21] or

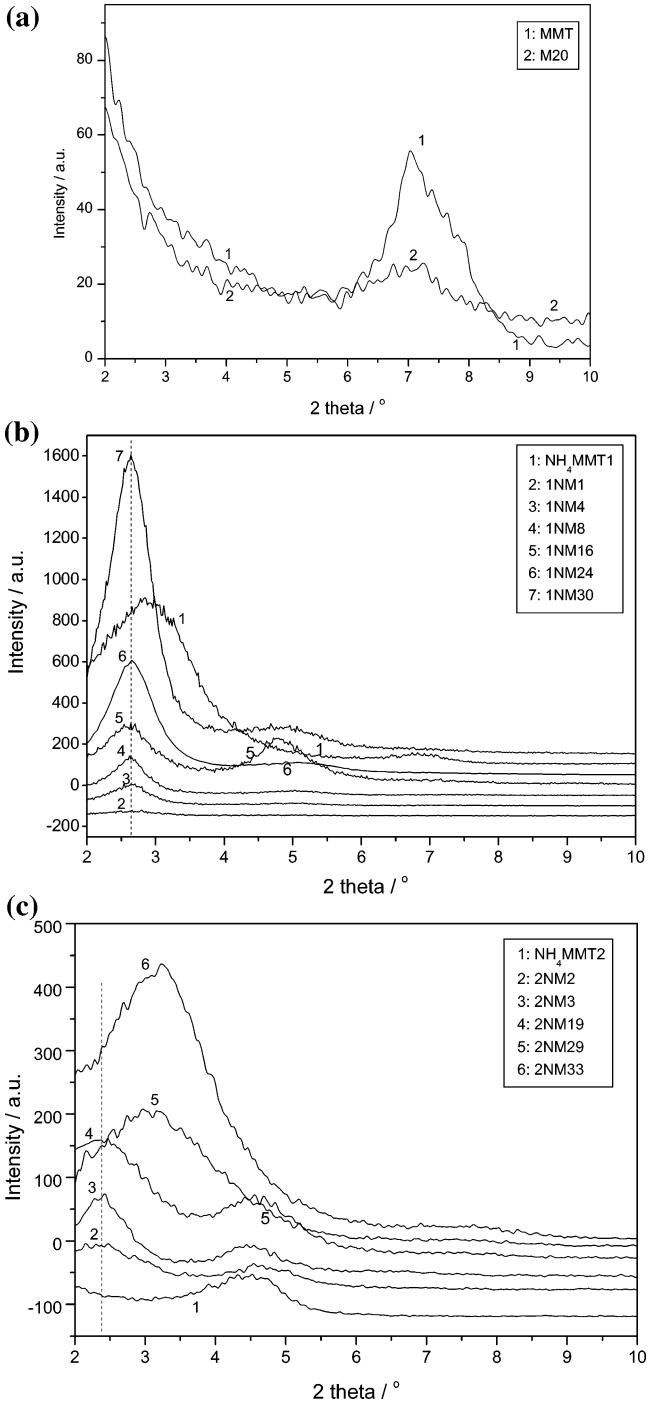

Figure 1. XRD traces of (a) PCL−natural montmorillonite (MMT), (b) PCL−ammonium-treated montmorillonite (NH_4MMT1), and (c) PCL−ammonium-treated montmorillonite (NH_4MMT2) composites.

"folded chain" structures.[20] Whichever conformation results, the amount of the intercalated polymer is assumed to be proportional to the increased interlayer spacing for subsequent effective volume fraction calculations.

With TEM, the microtomed PCL−clay conventional composites (PCL−MMT) only showed clay in the form of particles or agglomerates; discrete clay platelets were not seen even at high magnifications, confirming that the clay neither exfoliates nor intercalates. Ammonium-treated clays, e.g. sample 1NM1b (Figure 2a), clearly show clay platelets, mainly as intercalated clay tactoids with occasional exfoliated single platelets. The average number of clay platelets per stack is 5 with a 95% confidence interval of 0.4. This number was determined from

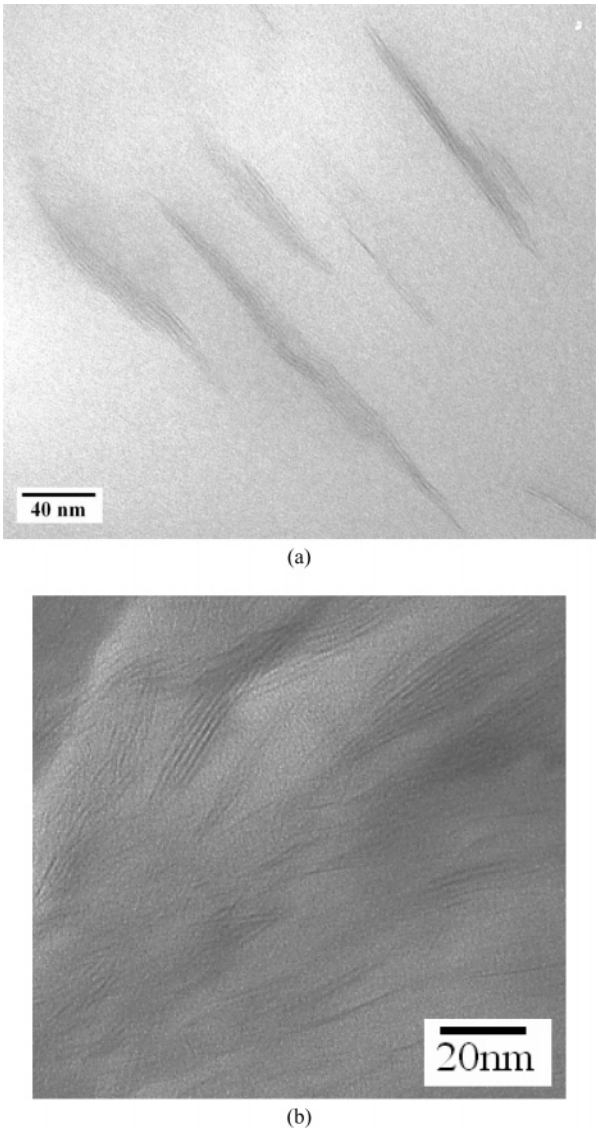

Figure 2. TEM images of (a) PCL−NH_4MMT1 (1NM1b) and (b) PCL−NH_4MMT2 (2NM3) composites.

20 stacks in the full TEM image, from which Figure 2a was cropped for clarity. Sample 1NM16, containing more clay, had tactoids with similar average thickness, suggesting a similar average number of clay platelets per stack. On the other hand, Figure 2b for sample 2NM3 shows stacks of clay layers and a large number of single platelets. The average number of clay platelets per stack (excluding single clay platelets) determined from a sample of 20 in Figure 2b was also 5 with a 95% confidence interval of 0.6. On the basis of these stack sizes, the effective volume fraction and modulus of the reinforcing phase for an intercalating system (PCL−NH_4MMT1) is calculated (vide infra). Although the same method can be applied where individual platelets are present (PCL−NH_4MMT2), this really requires a measurement of degree of exfoliation and a modified method for reinforcement volume fraction and modulus.

NMR spectra of PCL−clay composites are shown in Figure 3. The spectrum of PCL shows a carbonyl carbon resonance at 173.3 ppm and five methylene carbon resonances (64.9, 33.4, 28.5, 25.8, and 25.0 ppm) numbered from I to V and assigned to the carbons designated in Scheme 3.[22,23] The last two resonances (25.8 and 25.0 ppm) were very close and could not be distinguished in the spectra. Except for sample 1NM1b (with

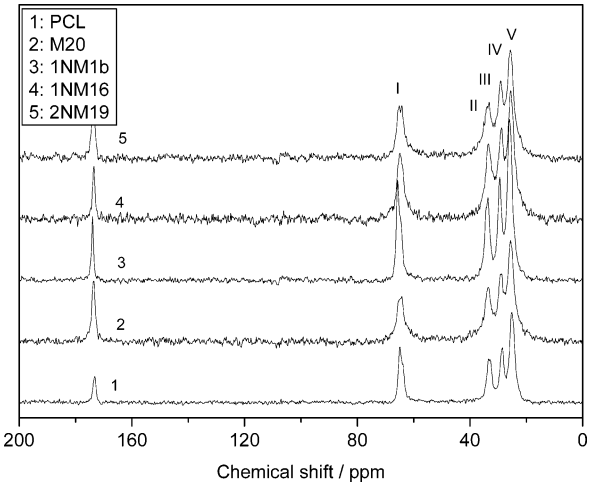

Figure 3. NMR spectra of PCL−clay composites.

Scheme 3. Identification of Carbons in ϵ-Caprolactone

-O-CH_2-CH_2-CH_2-CH_2-CH_2-CO-

I III V IV II

Table 2. DSC Data for PCL−Clay Composites

sample ID	T_{onset}/ °C	T_{peak}/ °C	enthalpy change[a]/ J g^{-1} PCL	crystallinity[b]/ %
PCL	48.5	54.8	54	40
M34	50.4	54.7	54	40
1NM1b	49.2	55.5	59	43
1NM4	52.4	59.6	58	43
1NM8	52.3	57.6	57	42
1NM16	51.8	56.3	50	37
2NM3	53.5	57.8	61	45
2NM19	51.5	57.6	52	38

[a] Based on mass of polymer. [b] Enthalpic change for 100% crystalline PCL = 136 J g^{-1}.[10,23]

2 wt % clay) having ∼1 ppm shift, all the other composites have almost the same peak positions. The greatest chemical shift suggests that PCL and NH_4MMT1 had the largest interaction, i.e., largest specific interfacial surface area between PCL and clay.

Table 2 summarizes the melting temperatures and enthalpy changes during melting for PCL−clay composites. The conventional composite (M34) had the same crystallinity as the unfilled polymer, namely 40% based on the value of 136 J g^{-1} for 100% crystallinity;[10,23] there were no significant nucleating effects. Ray et al.[16] found that only exfoliated silicate platelets act as effective nucleating agents causing smaller crystallite formation in PLA−organoclay nanocomposites.

Crystallinity of PCL in the nanocomposites first increased with increasing organoclay loading and then decreased. Exfoliated clay did act as a nucleating agent, increasing crystallinity as found by Gopakumar et al.[24] However, the polymer that intercalated into clay galleries becomes amorphous thus decreasing crystallinity.[25,26] These results suggest that at low organoclay loadings the nucleating effect played the major role, and at higher organoclay loadings, the intercalated polymer dominated the change of crystallinity.

When comparing PCL−NH_4MMT1 with PCL−NH_4MMT2 nanocomposites, the latter shows a greater increase in crystallinity, indicative of greater nucleating effects due to larger interfacial area between the clay and PCL. This is in agreement with the TEM images which show a greater degree of exfoliation for the PCL−NH_4MMT2 nanocomposite at the low clay loading.

Figure 4 shows the longitudinal modulus from ultrasonic pulse-echo testing as a function of clay mass fraction (corrected

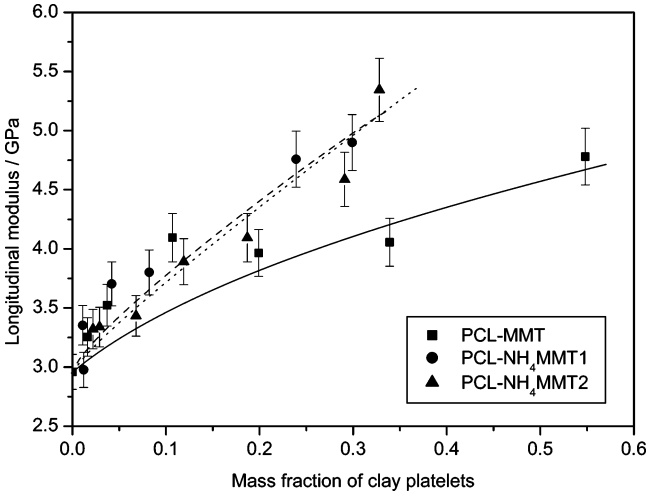

Figure 4. Longitudinal modulus vs mass fraction of clay platelets for PCL−clay composites measured by ultrasonic testing. The error bars refer to 5% measurement error as calibrated by a steel step-wedge.

Table 3. Tensile Strengths and Flexural Yield Strength of PCL−Clay Composites[a]

sample	tensile strength/MPa	flexural yield strength/MPa
PCL	17(0.5)	23(1.2)
M2	32(1.5)	26(1.7)
M4	22(0.4)	21(1.6)
M11	17(1.2)	27(0.8)
M20	15(1.4)	28(1.7)
M34	13(0.6)	30(0.3)
M45	12(0.7)	29(0.7)
M55	11(0.9)	26(1.3)
1NM1	27(2.2)	27(1.6)
1NM1b	27(2.5)	27(2.6)
1NM4	32(1.7)	30(3.2)
1NM8	31(2.2)	30(1.0)
1NM16	19(0.4)	29(2.3)
1NM24	15(0.7)	28(1.3)
1NM30	14(0.9)	22(1.6)
2NM2	29(0.9)	24(1.9)
2NM3	30(2.6)	24(0.9)
2NM7	32(1.0)	28(0.6)
2NM12	22(1.2)	29(1.2)
2NM19	21(1.9)	26(1.7)
2NM29	16(1.0)	24(2.1)
2NM33	14(0.2)	23(1.2)

[a] The numbers in parentheses refer to standard deviations.

for treated clay additives) for PCL−clay composites. Clay increases the elastic modulus regardless of clay type. The ammonium-treated clays provided a significantly greater increase than the natural clay because they formed nanocomposites with PCL with higher interfacial surface areas and greater effective volume fractions as discussed below. The curves for the two nanocomposites are indistinguishable.

The transverse wave was attenuated by PCL, and so shear modulus and hence the other elastic constants for composites with lower clay volume fractions were not obtained. However, the results for longitudinal modulus clearly show that the nanocomposites gave greater property enhancement than the conventional composites. The results from mechanical testing, as discussed below, support this conclusion.

Tensile strengths of the composites are summarized in Table 3. The tensile strength leveled off at higher loadings. This suggests that the external load could not be transferred effectively to the clay platelets when the clay was at high concentration, possibly due to the presence of clay agglomerates. Figure 5 shows the tensile elongation at break as a function of clay platelet loadings. At low clay loadings, test pieces

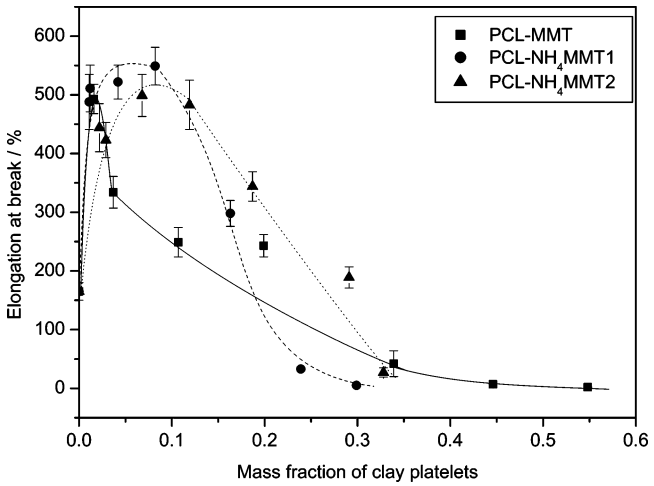

Figure 5. Tensile elongation at break as a function of clay platelet loadings for the PCL−clay composites.

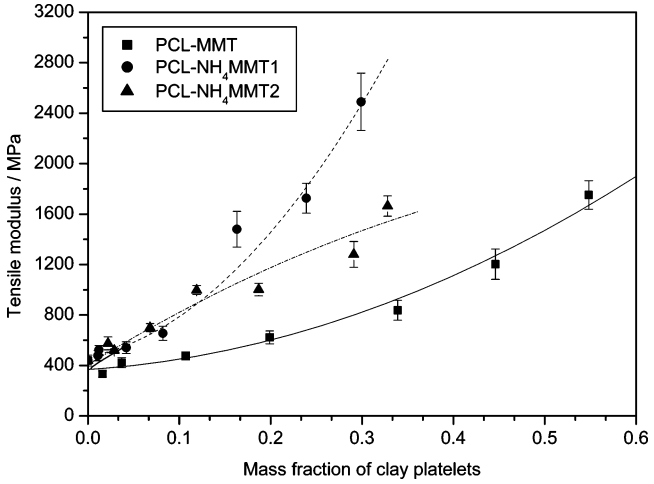

Figure 6. Young's modulus vs mass fraction of clay platelets for PCL−clay composites. The error bars refer to standard deviations.

underwent yielding during tension, similar to pristine PCL but with dramatic increases in ductility—quite the opposite of the usual effect of adding a particulate filler to a polymer. When the clay loading was high, typically greater than 20 wt % clay (i.e., M34, M45, M55, 1NM24, 1NM30, and 2NM33), the composites became brittle, there being no yielding stage in the stress−strain curve. The increase in tensile strength without sacrificing elongation at break provides these composites with very attractive mechanical properties, which have also been found by other workers in the nanocomposite field (e.g., refs 3, 6, and 27).

Figure 6 shows Young's modulus deduced from tensile tests vs mass fraction of clay platelets for PCL−clay composites. As with longitudinal modulus, the curves for the nanocomposites are above those for the conventional composites, indicating more effective reinforcement. At lower clay loadings (clay platelets <12 wt %), NH_4MMT2 gave a slightly higher modulus. Since TEM images (Figure 2) show that the PCL−NH_4MMT2 nanocomposite containing 1.2 wt % clay has more single clay platelets than PCL−NH_4MMT1, this result implies that composites with more exfoliation give greater property enhancement. To understand the property−volume fraction relationships requires the calculation of effective volume fraction of clay reinforcement and is discussed below.

Generally, nanocomposites appear to give more increase in the tensile strength and Young's modulus at a given loading

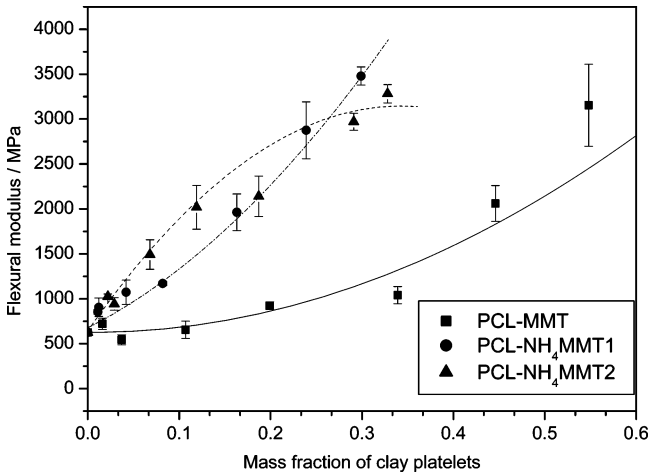

Figure 7. Flexural modulus vs mass fraction of clay platelets for PCL−clay composites. The error bars refer to standard deviations.

than do conventional composites. Taking sample 1NM4, which has a clay loading of 4.2 wt % platelets, a loading that is often reported in the literature for polymer−clay nanocomposites, as an example, the tensile strength, Young's modulus, and elongation at break of PCL were increased from 17 to 31 MPa, 439 to 655 MPa, and 165 to 522%, respectively. However, the conventional composite with a similar clay loading (3.7 wt %), namely sample M4, only had a modest increase in tensile strength and no increase in Young's modulus.

In flexural testing, the PCL−clay composites did not break at the flexural strain of 5%; thus, yield strengths rather than fracture strengths were obtained. Both nanocomposites gave steeper stress−strain curves than the conventional composite, indicating a greater flexural modulus. The flexural yield strengths are also given in Table 3. As with the results from tensile testing, the yield strength first increased with clay loading and then decreased, while the flexural modulus increased monotonically with increasing clay loadings.

Figure 7 shows the flexural modulus vs mass fraction of clay platelets for the PCL−clay composites deduced using the ASTM procedure but subject to the limitations of this type of measurement for an anelastic response. As in the results from tensile testing, the nanocomposites gave greater flexural moduli than the conventional composite with a similar loading. Again, NH_4-MMT2 gave more increase in the modulus after correction for clay platelet addition, supporting the conclusion that the nanocomposite with more exfoliation has a higher modulus. Similarly, taking sample 1NM4 (containing 4.2 wt % clay platelets) as the example, its yield strength and flexural modulus were increased from 23 to 30 MPa and from 625 to 1073 MPa, respectively, demonstrating substantial property enhancement.

SEM images of the fracture surfaces of PCL−MMT conventional composites (M20) and PCL−NH_4MMT2 nanocomposite (sample 2NM19) with similar platelet loadings are shown in Figure 8. In the conventional composite, bulk clay particles can be clearly seen in the micrograph, as indicated by the arrows. These particles do not appear in the nanocomposites.

(ii) Application of Composite Theory. *Volume Fractions of Nanocomposites.* The results expressed thus far are of interest in the commercial development of new biodegradable materials, but of fundamental importance is the relationship of these results to composite materials theory. Although it is useful in terms of materials development to express modulus in terms of wt % clay, an understanding of how nanocomposites fit into general composite theory should be obtained by expressing properties

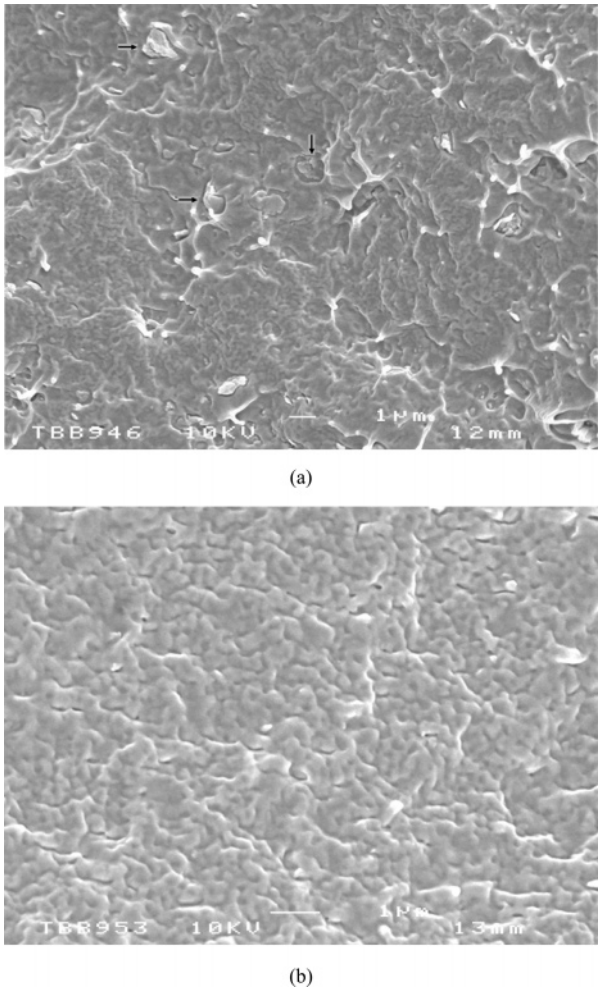

Figure 8. SEM images of fracture surfaces for (a) PCL−MMT conventional composite (M20) and (b) PCL−NH_4MMT2 nanocomposite (2NM19). Arrows point to bulk clay particles.

in terms of volume fraction of dispersed phase. Thus, before proceeding to interpret mechanical data in terms of composition and structure, effective volume fractions of reinforcement in the nanocomposites were calculated as described below.

Since natural montmorillonite retained its structure after melt-processing, its effective volume fractions in the PCL−MMT conventional composites can be directly calculated from weight percents of clay (column 2, Table 1) and the densities of PCL and MMT. The results are listed in column 3 of Table 1. However, in nanocomposites, the volume fraction of clay particles increases after the intercalation of polymer molecules and the free interstitial polymer decreases correspondingly, and it is the intercalated clay tactoid that plays the role of reinforcement filler. Assuming PCL molecules occupy the increased gallery spacing of the organoclay based on the models proposed by Okada et al.[2] and LeBaron et al.,[6] the effective volume fractions of reinforcement for the nanocomposites can be calculated as follows:[28]

$$\frac{1}{\phi_c^i} = 1 + \frac{\rho_c'(1 - \mu_c' - \mu_c'\mu_c^0 s)[d_1'(N-1) + h]}{\mu_c'\rho_p[d_2(N-1) + h]} \quad (1)$$

where d_1' and d_2 are the basal plane spacings of unfilled and filled organoclay, respectively; N is the average number of clay platelets per stack; h is the thickness of a clay platelet, which is 0.98 nm;[29] ρ_p and ρ_c' are the densities of PCL and the organoclay, which are 1140 and 1700 kg m^{-3}, respectively; s is the ratio of the intercalated polymer to clay; μ_c^0 is the mass fraction of inorganic component in the organoclay and is 62.2 wt % for NH_4MMT1 and 77.8 wt % for NH_4MMT2 according to loss on ignition; and μ_c' is the original mass fraction of the organoclay in the mixture (column 2, Table 1).

The average number of clay platelets per stack N was taken as 5 for all the composites. The uptake ratio is unknown for PCL, but ϕ_c^i is insensitive to s so that when $s = 0.06$ or 0.2 g g^{-1} clay per layer, the effective volume fractions of reinforcement in PCL−NH_4MMT1 nanocomposites are unchanged for all but the three highest loadings where the deviations are no greater than 2 vol %. Making the assumption that s is proportional to the polymer layer number, $s = 0.06$ and 0.2 g g^{-1} per layer are the minimum and maximum bilayer data, respectively, according to the literature for poly(ethylene oxide)s (PEO),[26,30] i.e., 0.11 g g^{-1} for PEO−NH_4MMT nanocomposites and 0.39 (by XRD and DSC) g g^{-1} for PEO−MMT nanocomposites. Indeed, a deviation of 5 vol % for the highest loading is produced only if s is increased to 0.35 g g^{-1} clay per layer. Thus, $s = 0.06$ g g^{-1} per layer is taken for the following calculation. For NH_4MMT1, the increment in d_{001} was 0.4 nm (monolayer), and the calculated effective volume fractions are listed in column 3 of Table 1. For NH_4MMT2, the increments in d_{001} were 1.6 nm (quadlayer) except for samples 2NM29 and 2NM33, for which it was 0.8 nm (bilayer); thus, $s = 0.24$ g g^{-1} was taken for samples 2NM2−2NM19 and $s = 0.12$ g g^{-1} for samples 2NM29 and 2NM33. The calculated effective volume fractions are also listed in Table 1.

Elastic Moduli of Conventional Composites. The data for conventional nanocomposites were compared using established equations for particle-reinforced composites, noting that these refer to spherical inclusions. Since polymer did not enter into clay galleries, the near-spherical bulk clay particles act as the reinforcement filler. Thus, shear modulus and bulk modulus of the reinforcement filler were those for bulk montmorillonite, namely 5.5 and 11 GPa, respectively.[31] The Young's modulus of PCL was 0.44 GPa using the value from tensile testing. The longitudinal modulus of PCL was 2.96 GPa as measured by ultrasonic testing. Since $L = E/3(1 - 2\upsilon) + 2E/3(1 + \upsilon)$, Poisson's ratio υ of the unfilled PCL is calculated to be 0.47, which is consistent with the Poisson's ratios for samples M55, 1NM30, and 2NM33, namely 0.36, 0.42, and 0.40 obtained solely from ultrasonic testing. Young's modulus measured from tensile testing is slightly lower than that measured from ultrasonic testing in a material with an anelastic response because of the low strain in ultrasound transmission.

Shear and bulk moduli of each conventional composite were calculated using Benveniste's model[32] being identical to Christensen's model[33] for bulk modulus:

$$K = K_2 + \frac{(K_1 - K_2)c_1}{1 + (K_1 - K_2)(1 - c_1)/\left(K_2 + \frac{4}{3}G_2\right)} \quad (2)$$

$$G = G_2 + \frac{(G_1 - G_2)c_1}{1 + (G_1 - G_2)(1 - c_1)/\left[G_2 + \frac{G_2(9K_2 + 8G_2)}{6(K_2 + 2G_2)}\right]} \quad (3)$$

where c is the volume fraction. Subscripts 1 and 2 refer to reinforcement and matrix, respectively. These two equations are the lower Hashin−Shtrikman (H−S) bounds,[34] as already noted by Christensen.[33] Young's modulus was calculated according

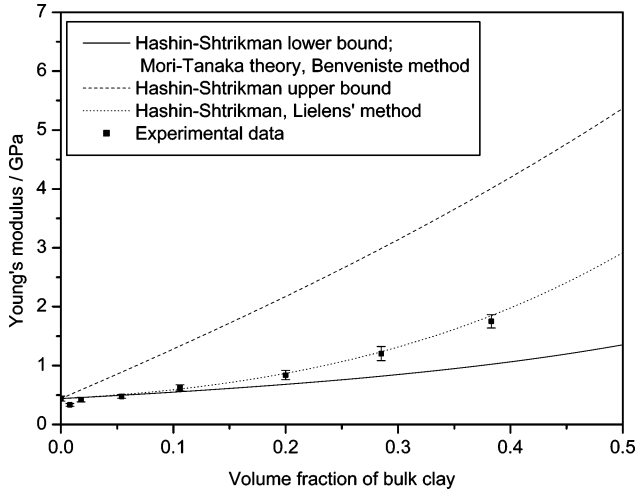

Figure 9. Young's modulus vs volume fraction of clay for PCL−MMT conventional composites.

to eq 4 and is plotted as a function of volume fraction in Figure 9.

$$E = 9KG/(3K + G) \tag{4}$$

Figure 9 shows the experimental data fall between the Hashin−Shtrikman bounds.[34] The H−S−Lielens method[35] applies a coefficient related to the volume fraction of the reinforcement filler, $(c_1 + c_1^2)/2$, to the upper and lower Hashin−Shtrikman bounds, and the values of the moduli for composites determined in this way agree with the experimental data very well. This method has been deemed successful by others.[36]

Elastic Moduli of Treated-Clay Nanocomposites: Type 1. In PCL−clay nanocomposites, the reinforcement filler is made up of polymer and the organoclay containing quaternary ammonium molecules and clay platelets. Young's modulus of clay platelets was taken as 178 GPa in accordance with the measured value for mica[37,38] which has a similar crystalline structure, this value being used in several studies.[39,40] Poisson's ratio was taken as 0.28 according to the measured values for mullite ($3Al_2O_3 \cdot 2SiO_2$),[41,42] sillimanite ($Al_2O_3 \cdot SiO_2$),[41] kaolinite,[43] and montmorillonite.[43] The modulus of the ammonium surfactant was taken as that for PCL on the basis that clay platelets provide a much higher modulus than the organic matter, being 178 GPa compared to a modulus less than 1 GPa. Using Christensen's equations for two-dimensional platelet-filled systems,[44] as given by eqs 5 and 6, for calculating the intercalated clay tactoids and assuming the organic molecules occupy the full gallery spacing of the intercalated clay, the elastic moduli and Poisson's ratio for the intercalated tactoids can be calculated.

$$G = \frac{1}{h}(h_1G_1 + h_2G_2) \tag{5}$$

$$E = c_1E_1 + c_2E_2 + \frac{c_1c_2E_1E_2(\upsilon_1 - \upsilon_2)^2}{c_1E_1(1 - \upsilon_2^2) + c_2E_2(1 - \upsilon_1^2)} \tag{6}$$

where $h = h_1 + h_2$; h_1 and h_2 are the thicknesses of the two alternating materials, respectively. Subscripts 1 and 2 refer to the reinforcement filler and matrix, respectively. c is the volume fraction, and $c_1 = h_1/h$, $c_2 = h_2/h$. In this type of nanocomposite, $h_1 = 0.98$ nm and $h = 3.5$ nm. Hence $c_1 = 0.28$ and $c_2 = 0.72$. Inserting the data into eqs 5 and 6, the elastic constants of the intercalated clay tactoids are obtained, which are shown in Table 4.

Table 4. Effective Elastic Constants of the Intercalated Clay Tactoids Acting as the Reinforcement Filler in PCL−NH_4MMT Nanocomposites, Deduced Using Christensen's Method for Platelet-Filled Composites

filler ID	Young's modulus/GPa	shear modulus/GPa	bulk modulus/GPa	Poisson's ratio
PCL−NH_4MMT1	50.2	19.6	38.0	0.28
PCL−NH_4MMT2a[a]	48.4	18.9	36.7	0.28
PCL−NH_4MMT2b[b]	62.6	24.4	47.4	0.28

[a] For samples 2NM2−2NM19. [b] For samples 2NM29 and 2NM33.

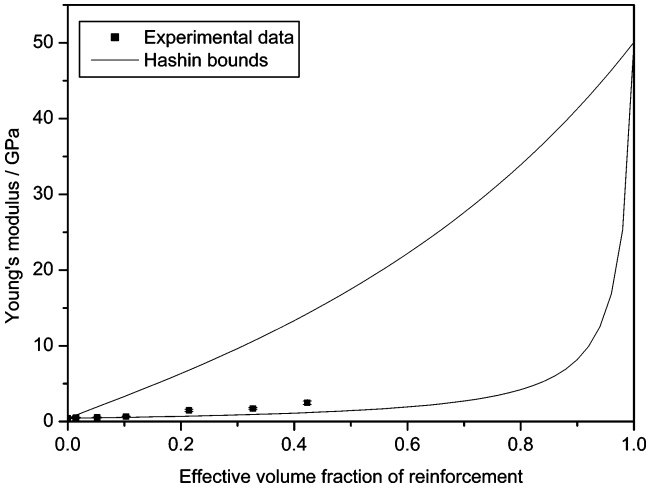

Figure 10. Young's modulus vs effective volume fraction of reinforcement for PCL−NH_4MMT1 nanocomposites.

Thus, the lower H−S bound (cf. eqs 2 and 3) of the PCL−NH_4MMT1 nanocomposites can be calculated using the data described above and is shown in Figure 10. Exchanging the subscripts 1 and 2 in eqs 2 and 3 yields the upper H−S bounds for bulk modulus and shear modulus. Figure 10 shows that the experimental data fall between the H−S bounds and are very close to the lower bound, which is often true for binary-phase composites with fillers having much higher moduli.[45−48]

Elastic Moduli of Treated-Clay Nanocomposites: Type 2. The elastic constants of the intercalated clay tactoids for PCL−NH_4-MMT2 nanocomposites can be calculated in the same way as in type 1. h_1 again is 0.98 nm, but the value of h is changed because of the different basal plane spacings in the nanocomposites. For samples 2NM2−2NM19, $h = 3.6$ nm; hence $c_1 = 0.27$ and $c_2 = 0.73$. For samples 2NM29 and 2NM33, $h = 2.8$ nm; hence $c_1 = 0.35$ and $c_2 = 0.65$. The results are also shown in Table 4.

Figure 11 shows the experimental data and the theoretical data predicted using the H−S bounds. Again, Young's moduli of the nanocomposites are within the H−S bounds and are also very close to the lower H−S bounds, as they were in the case of PCL−NH_4MMT1 nanocomposites. These composite modulus calculations are based on the method for fully intercalated nanocomposites. TEM shows that this is a reasonable approach for PCL−NH_4MMT1 where clay tactoids were observed, but few individual single platelets were seen. However, when there is a significant population of single platelets, as is the case in PCL−NH_4MMT2, the system needs to be treated as an intercalated−exfoliated nanocomposite[28] for which a reliable method of finding the overall exfoliation extent is first required.

It appears that if the effective volume fractions of reinforcement in nanocomposites are calculated, the results of elastic modulus can be interpreted using the elastic modulus−volume fraction models for conventional composites provided that the elastic modulus of the reinforcement can be estimated. At a

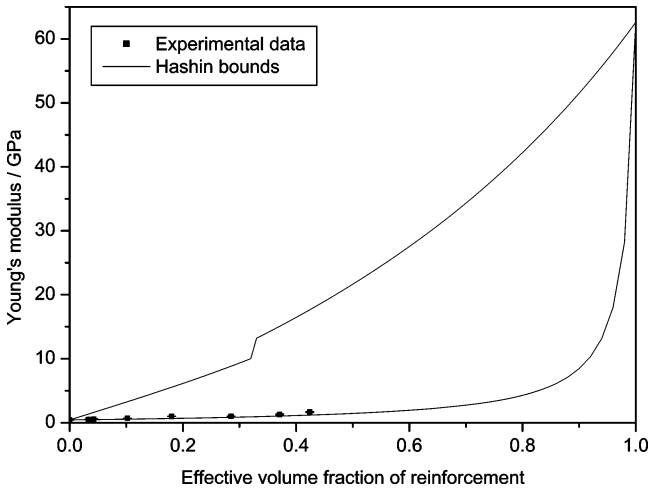

Figure 11. Young's modulus vs effective volume fraction of reinforcement for PCL−NH_4MMT2 nanocomposites. The transition point refers to the volume fraction where the basal plane spacing of the intercalated clay changes.

given clay loading, the PCL nanocomposites had superior mechanical properties to the conventional composite. Besides the elastic modulus and volume fraction of the reinforcement, other factors such as crystallinity, orientation, bridging molecules between clay tactoids, and degree of exfoliation also affect elastic modulus. Thus, the relatively high elastic modulus for the PCL−NH_4MMT2 nanocomposites at low clay loadings could also be attributed to the greater crystallinity, as shown in Table 2, as well as the high elastic modulus of the reinforcement, as discussed above. Both are the result of the greater exfoliation degree in the PCL−NH_4MMT2 nanocomposites, which confirms the view that nanocomposites with more exfoliation provide a higher elastic modulus than those which are predominantly intercalated for the same mass fraction of clay.

Conclusions

PCL−clay composites with three types of montmorillonite and clay loadings ranging from 1.7 to 59 wt % were prepared by melt-processing. The natural montmorillonite formed conventional composites with PCL as evidenced by XRD and TEM. Both ammonium-treated montmorillonites formed nanocomposites but with slightly different microstructures. DSC results show that the crystallinity of PCL was increased when the organoclay loading was low, and it was decreased with higher clay loadings. The crystallinity of PCL in the conventional composites was not changed.

The presence of clay in PCL increased the longitudinal modulus, tensile strength, tensile modulus, flexural yield strength, and flexural modulus and afforded dramatic improvements in elongation at break. When the clay loading was typically lower than 30 wt %, the PCL−clay composites were ductile and experienced yielding during mechanical testing. Generally the nanocomposites had a higher strength or modulus than the conventional composites with similar clay loadings, and the nanocomposite with more exfoliation provided a greater increase in the strength or modulus than the one with less exfoliation. All the experimental data for elastic modulus in nanocomposites fall between the H−S bounds and are very close to the lower H−S bound, suggesting that the elastic modulus−volume fraction relationships in nanocomposites can be interpreted using well-established theory for conventional composites.

Acknowledgment. This work is supported by the Engineering and Physical Sciences Research Council in the U.K. under Grant GR/T24166. We are grateful to Dr. Harold Toms (Department of Chemistry) for operating the NMR instrument.

References and Notes

(1) Usuki, A.; Kojima, Y.; Kawasumi, M.; Okada, A.; Fukushima, Y.; Kurauchi, T.; Kamigato, O. *J. Mater. Res.* **1993**, *8*, 1179−1184.
(2) Okada, A.; Usuki, A. *Mater. Sci. Eng., C* **1995**, *3*, 109−115.
(3) Pinnavaia, T. J.; Beall, G. *Polymer-Clay Nanocomposites;* John Wiley & Sons Ltd.: Chichester, 2000.
(4) Vaia, R. A.; Jandt, K. D.; Kramer, E. J.; Giannelis, E. P. *Macromolecules* **1995**, *28*, 8080−8085.
(5) Aranda, P.; Ruiz-Hitzky, E. *Appl. Clay Sci.* **1999**, *15*, 119−135.
(6) LeBaron, P. C.; Pinnavaia, T. J. *Chem. Mater.* **2001**, *13*, 3760−3765.
(7) Jinadasa, K. B. P. N.; Dissanayake, C. B. *Environ. Geochem. Health* **1992**, *14*, 3−7.
(8) Bakraji, E. H.; Karajou, J. *J. Trace Microprobe Tech.* **2003**, *21*, 397−405.
(9) Pang, J. T.; Fan, C. H.; Liu, X. J.; Chen, T.; Li, G. X. *Biosens. Bioelectron.* **2003**, *19*, 441−445.
(10) Lepoittevin, B.; Devalckenaere, M.; Pantoustier, N.; Alexandre, M.; Kubies, D.; Calberg, C.; Jerome, R.; Dubois, P. *Polymer* **2002**, *43*, 4017−4023.
(11) Gorrasi, G.; Tortora, M.; Vittoria, V.; Galli, G.; Chiellini, E. *J. Polym. Sci., Part B* **2002**, *40*, 1118−1124.
(12) Gorrasi, G.; Tortora, M.; Vittoria, V.; Pollet, E.; Lepoittevin, B.; Alexandre, M.; Dubois, P. *Polymer* **2003**, *44*, 2271−2279.
(13) Tortora, M.; Vittoria, V.; Galli, G.; Ritrovati, S.; Chiellini, E. *Macromol. Mater. Eng.* **2002**, *287*, 243−249.
(14) Chen, B.; Evans, J. R. G. *Carbohydr. Polym.* **2005**, *61*, 455−463.
(15) Chen, M.; Chen, B.; Evans, J. R. G. *Nanotechnology* **2005**, *16*, 2334−2337.
(16) Ray, S. S.; Yamada, K.; Okamoto, M.; Fujimoto, Y.; Ogami, A.; Ueda, K. *Chem. Mater.* **2003**, *15*, 1456−1465.
(17) Dixon, W. T.; Schaefer, J.; Sefcik, M. D.; Stejskal, E. O.; McKay, R. A. *J. Magn. Reson.* **1982**, *49*, 341−345.
(18) Chen, B.; Evans, J. R. G. *Polym. Int.* **2005**, *54*, 807−813.
(19) Chen, B. *Br. Ceram. Trans.* **2004**, *103*, 241−249.
(20) Triantafillidis, C. S.; LeBaron, P. C.; Pinnavaia T. J. *J. Solid State Chem.* **2002**, *167*, 354−362.
(21) Ruiz-Hitzky, E.; Aranda, P. *Adv. Mater.* **1990**, *2*, 545−547.
(22) Clark, M. B.; Burkhardt, C. A.; Gardella, J. A. *Macromolecules* **1989**, *22*, 4495−4501.
(23) de Kesel, C.; Lefevre, C.; Nagy, J. B.; David, C. *Polymer* **1999**, *40*, 1969−1978.
(24) Gopakumar, T. G.; Lee, J. A.; Kontopoulou, M.; Parent, J. S. *Polymer* **2002**, *43*, 5483−5491.
(25) Vaia, R. A.; Sauer, B. B.; Tse, O. K.; Giannelis, E. P. *J. Polym. Sci., Part B* **1997**, *35*, 59−67.
(26) Shen, Z.; Simon, G. P.; Cheng, Y.-B. *Eur. Polym. J.* **2003**, *39*, 1917−1924.
(27) Park, H.-W.; Lee, W.-K.; Park, C.-Y.; Cho, W.-J.; Ha, C.-S. *J. Mater. Sci.* **2003**, *38*, 909−915.
(28) Chen, B.; Evans, J. R. G. Submitted to *Macromolecules*.
(29) Chen, B.; Evans, J. R. G. *J. Phys. Chem. B* **2004**, *108*, 14986−14990.
(30) Chen, B.; Evans, J. R. G. *Philos. Mag.* **2005**, *85*, 1519−1538.
(31) Prasad, M. *Geophys. Res. Lett.* **2002**, *29*, 13−1−13−4.
(32) Benveniste, Y. *Mech. Mater.* **1987**, *6*, 147−157.
(33) Christensen, R. M. *J. Mech. Phys. Solids* **1990**, *38*, 379−404.
(34) Hashin, Z.; Shtrikman, S. *J. Mech. Phys. Solids* **1963**, *11*, 127−140.
(35) Lielens, G.; Pirotte, P.; Couniot, A.; Dupret, F.; Keunings, R. *Composites A* **1998**, *29*, 63−70.
(36) Tucker, C. L.; Liang, E. *Compos. Sci. Technol.* **1999**, *59*, 655−671.
(37) McNeil, L. E.; Grimsditch, M. *J. Phys.: Condens. Matter* **1993**, *5*, 1681.
(38) Vaughan, M. T.; Guggenheim, S. *J. Geophy. Res. B* **1986**, *91*, 4657.
(39) Kornmann, X.; Berglund, L. A.; Sterte, J.; Giannelis, E. P. *Polym. Eng. Sci.* **1998**, *38*, 1351.
(40) Zhu, L.; Narh, K. A. *J. Polym. Sci., Part B* **2004**, *42*, 2391.
(41) Hildmann, B.; Ledbetter, H.; Kim, S.; Schneider, H. *J. Am. Ceram. Soc.* **2001**, *84*, 2409−2414.
(42) Ledbetter, H.; Kim, S.; Balzar, D. *J. Am. Ceram. Soc.* **1998**, *81*, 1025−1028.
(43) Vanorio, T.; Prasad, M.; Nur, A. *Geophys. J. Int.* **2003**, *155*, 319−326.
(44) Christensen, R. M. *Mechanics of Composite Materials;* John Wiley & Sons: New York, 1979; pp 46−48, 100−144.
(45) Peng, H. X. *Mater. Sci. Eng., A* **2005**, *396*, 1−2.
(46) Wong, C. P.; Bollampally, R. S. *J. Appl. Polym. Sci.* **1999**, *74*, 3396−3403.
(47) Peng, H. X.; Fan, Z.; Evans, J. R. G. *Mater. Sci. Eng., A* **2001**, *303*, 37−45.
(48) Zhao, M.; Wu, G. H.; Dou, Z.; Zhang, L. T. *Mater. Sci. Eng., A* **2004**, *374*, 303−306.

MA052154A